ACADEMIC PRESS

Available online at www.sciencedirect.com

SCIENCE DIRECT®

Journal of Sound and Vibration 267 (2003) 537–548

JOURNAL OF SOUND AND VIBRATION

www.elsevier.com/locate/jsvi

# Numerical prediction of rail roughness growth on tangent railway tracks

J.C.O. Nielsen*

*Department of Applied Mechanics/CHARMEC, Chalmers University of Technology, SE-412 96 Gothenburg, Sweden*

Accepted 9 May 2003

**Abstract**

Growth of railhead roughness (irregularities, waviness) is predicted through numerical simulation of dynamic train–track interaction on tangent track. The hypothesis is that wear is caused by longitudinal slip due to driven wheelsets, and that wear is proportional to the longitudinal frictional power in the contact patch. Emanating from an initial roughness spectrum corresponding to a new or a recent ground rail, an initial roughness profile is determined. Wheel–rail contact forces, creepages and wear for one wheelset passage are calculated in relation to location along a discretely supported track model. The calculated wear is scaled by a chosen number of wheelset passages, and is then added to the initial roughness profile. Field observations of rail corrugation on a Dutch track are used to validate the simulation model. Results from the simulations predict a large roughness growth rate for wavelengths around 30–40 mm. The large growth in this wavelength interval is explained by a low track receptance near the sleepers around the pinned–pinned resonance frequency, in combination with a large number of driven passenger wheelset passages at uniform speed. The agreement between simulations and field measurements is good with respect to dominating roughness wavelength and annual wear rate. Remedies for reducing roughness growth are discussed.


## 1. Introduction

High-frequency vertical wheel–rail contact forces together with vibrations and rolling noise are induced when a train runs on a tangent track with irregularities (roughness, waviness) on the running surfaces of wheels and rails. Short pitch rail corrugation (roaring rails) with wavelengths in the range 25–80 mm is a severe example of such an irregularity. The present study was performed within the Brite/EuRam III project 'Silent Track', where the main objective was to

*Tel.: +46-31-772-1500; fax: +46-31-772-3827.
*E-mail address:* jens.nielsen@me.chalmers.se (J.C.O. Nielsen).

0022-460X/$ - see front matter © 2003 Elsevier Ltd. All rights reserved.
doi:10.1016/S0022-460X(03)00713-2

reduce rolling noise from the track through the design of acoustically optimized track components. An efficient approach to reduce rolling noise would be to find measures to delay, or preferably to avoid, the growth of rail roughness.

The great diversity of rail corrugation is an enigma that has puzzled railway researchers for more than a century. Rail corrugation occurs on most types of track including those in subways, on high-speed and heavy-haul lines, on tangent tracks and on curves. Corrugation wavelengths may vary from 25 to 1500 mm. Extensive state-of-the-art papers on the subject have been written by Grassie and Kalousek [1,2] and Knothe [3]. In Ref. [1,2], different types of corrugation are first classified with respect to damage and wavelength-fixing mechanisms. Treatments to avoid or reduce the problem are then proposed. Although causes of many types of corrugation are known, rail grinding remains the most widely used treatment.

The paper will focus on short pitch rail corrugation on tangent track. An example from the Netherlands is used as a case study. Here corrugation with dominating wavelengths in the range 30–40 mm and vertical peak-to-peak deviation around 40 μm has been observed. In a companion paper [4], the test site is described in detail and metallurgical investigations of a rail sample taken from the track are reported. According to Knothe [3], validations of integrated mathematical models (including the dynamic train–track interaction and the long-term wear of the railhead) compared to field observations have not previously been published. In the present paper, such a validation is attempted. Since the present study was performed in order to find means to reduce rolling noise, it was more important to predict the roughness level spectrum than the actual roughness profile.

## 2. Mathematical models for prediction of rail corrugation

Most mathematical models adopted to predict rail corrugation include (1) a model of dynamic train–track interaction in order to determine forces and creepages in the wheel–rail contact patch, and (2) a wear model to account for the long-term wear process of the railhead surface.

### *2.1. Wavelength-fixing mechanisms*

An initial railhead irregularity is assumed, often in the form of a spectrum with wavelengths in a relevant range (5–100 mm for short pitch rail corrugation). The irregularity acts as input to the dynamic train–track system, which results in fluctuating (normal and tangential) contact forces, creepages and contact patch dimensions. A commonly applied hypothesis is that the material volume removed due to wear is proportional to the frictional power in the contact patch. Simulation of the dynamic interaction will reveal that wheel–rail contact forces and frictional power are higher at certain frequencies than at others. For a certain train speed, this means that wear will be higher at certain wavelengths. This is referred to as the wavelength-fixing mechanism. After millions of wheelset passages, a regular wear pattern referred to as short pitch rail corrugation may form. Common wavelength-fixing mechanisms that occur for different types of corrugation are resonances of the coupled train–track system (e.g., the P2 resonance) and the pinned–pinned resonance of the discretely supported rail [1,2].

### 2.2. Damage mechanism

Several different damage mechanisms have been suggested to be the cause of rail corrugation, such as wear, plastic deformation and rolling contact fatigue [1–3]. In most corrugation models [5–9], wear is the only assumed active damage mechanism. However, repeated normal and tangential loading will lead to elastic or elastic–plastic behaviour of the railhead. If plastic deformation occurs, this will result in residual stresses and probably work hardening. It is possible that plastic deformation counteracts the formation of corrugation due to wear if normal contact pressures are higher near the corrugation peaks than in the troughs [3,5,10]. White-etching layers (WEL) may form especially on the corrugation peaks. The WEL is hard and brittle, and it appears that the wear resistance on the corrugation peaks is twice as high as in the troughs [3]. Therefore if WEL exists, the wear resistance along the rail is locally dependent. Propagation of rolling contact fatigue cracks can lead to loss of fragments from the railhead. An area where the density of railhead fractures is high will form a corrugation trough [1].

## 3. Description of a corrugated test site

The tangent track investigated is located between Amersfoort and Baarn in the Netherlands. The track was reconstructed in 1978 and it has not been ground since then. Track design includes continuously welded UIC54 rails on FC9 rail pads (4.5 mm thick cork/rubber pads) and bi-bloc concrete sleepers. The nominal train speed is 130 km/h for passenger trains and 80 km/h for freight trains. The trains operate at constant speed since there are no stations nearby. Approximately 85% (200,000) of all driven wheelsets passing the test site each year are fitted on either DDM or ICM passenger trains. The test site is described in more detail in Ref. [4].

A well-documented data set on roughness growth since the early 1990s is available. Annually measured roughness level spectra from 1996 to 2000 are illustrated in Fig. 1(a). For all

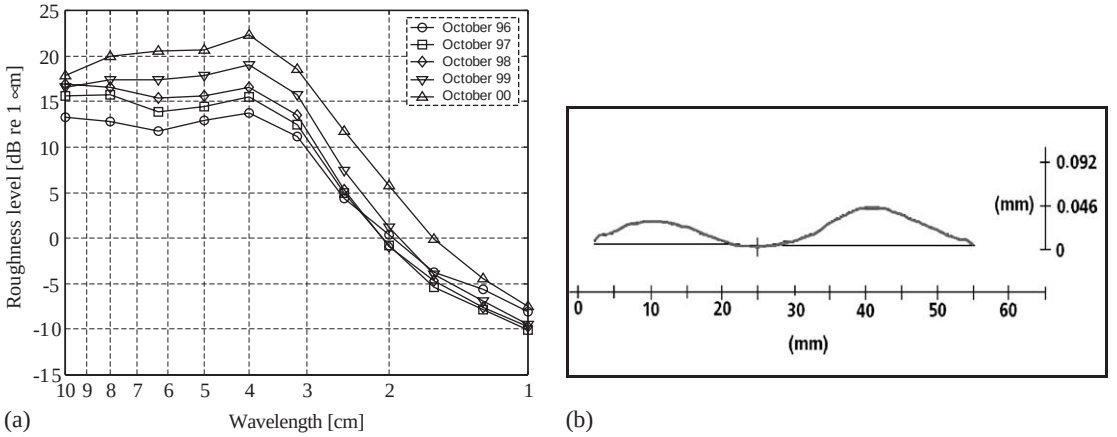


Fig. 1. (a) Annually measured roughness level spectra evaluated in 1/3 octave bands (roughness level is defined in Eq. (1)). (b) Longitudinal line scan of railhead surface indicating amplitude and wavelength of corrugation on sample taken from track.

wavelengths above 20 mm, there is a continuous growth of roughness amplitudes from year to year. The dominating wavelength around 40 mm with an average annual amplitude growth rate of around 25% (2 dB) is the most striking observation. The roughness profiles analyzed in Fig. 1(a) were measured using a RM1200E from Müller-BBM. Each calculated spectrum is a spectral average of 10 measured profile lines (length of each line = 1.2 m). On each rail, five lines were measured along a continuous distance of 6 m with no overlap. Fig. 1(b) illustrates a longitudinal line scan of the railhead measured on a 60 mm sample taken from the test site. Here, the measured maximum vertical deviation (peak-to-peak) was 41 μm and the wavelength was 30–35 mm.

## 4. Dynamic train–track interaction

Dynamic train–track interaction is either solved in the frequency domain or in the time domain. When the interaction is solved in the frequency domain, the included models must be linear. This means that they are limited to investigation of the initiation of roughness growth and low roughness amplitudes. However, solution times are short compared to time domain methods. Moving irregularity models where the vehicle is stationary at a given position along the track are used. The corrugation prediction models developed by Frederick [5] and Hempelmann [6] are examples from this model category. Time domain models can account for non-linear contact mechanics, state-dependent and randomized track properties, and they may be used to study both initiation and continued growth of rail corrugation. Moving mass models, where the vehicle is moving along the track at a given speed, are adopted. Examples in this category are the two models developed by Igeland and Ilias [7–9]. The present study is based on the work by Igeland, and on the procedure to solve dynamic train–track interaction that is described in Ref. [11].

The train–track interaction model is illustrated in Fig. 2. The rail is described by use of undamped Rayleigh–Timoshenko beam finite elements accounting for shear deformation and rotational inertia. Sleepers are treated as rigid masses. A constant sleeper spacing and track properties that are symmetric with respect to a centreline between the two rails are assumed. To shorten computation times, the loading on the track (including the roughness profile) is also taken as symmetric. This means that only half the track needs to be modelled. The length of the track model is 50 sleeper bays with clamped boundaries at the two rail ends. Only vertical track vibration is considered. Rail pads and ballast/ground in the discretely supported track model are modelled as two separate layers of linear springs and viscous dampers. Stiffnesses and viscous dampings were obtained by tuning the calculated direct vertical mobility (velocity divided by force) of the railhead above a sleeper to the corresponding mobility measured at the test site. The

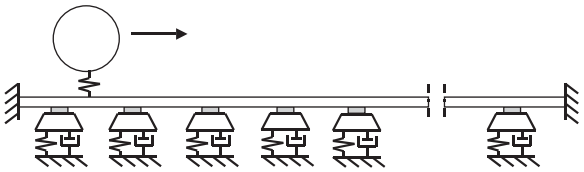

Fig. 2. Schematic illustration of mathematical model for vertical dynamic interaction between wheelset and railway track including wheel–rail contact stiffness.

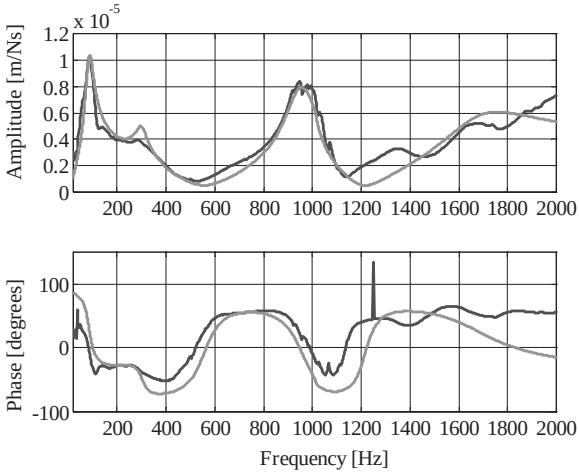


Fig. 3. Amplitude and phase of measured (black) and calculated (grey) direct track mobility of rail above sleeper.

Table 1
Summary of track and train properties

| Track component | Parameter | Value | Train model | Parameter | Value |
|---|---|---|---|---|---|
| UIC 54 rail | Bending stiffness | 4.5 MN m$^2$ | Passenger train ICM-III | Unsprung mass | 1800 kg |
| | Shear stiffness | 224 MN | | Polar moment of inertia | 100 kg m$^2$ |
| | Mass | 54.4 kg/m | | Wheel diameter | 0.95 m |
| | Rotational inertia | 0.167 kg/m | | Axle load | 200 kN |
| | | | | Train speed | 130 km/h |
| Rail pad | Stiffness | 1.3 GN/m | | Traction force/wheel | 1500 N |
| | Viscous damping | 45 kN s/m | | | |
| | Side length | 0.16 m | 'Freight locomotive 1700' | Unsprung mass | 2400 kg |
| Sleeper | Mass | 244 kg | | Polar moment of inertia | 280 kg m$^2$ |
| | Sleeper distance | 0.60 m | | Wheel diameter | 1.20 m |
| | | | | Axle load | 200 kN |
| Ballast properties per railseat | Stiffness | 45 MN/m | | Train speed | 80 km/h |
| | Viscous damping | 32 kNs/m | | Traction force/wheel | 3000 N |

agreement between measured and calculated mobilities is illustrated in Fig. 3. Track properties are listed in Table 1.

The first resonance frequency in Fig. 3 is around 70 Hz. At this resonance, rail and sleepers are vibrating in phase on the ballast. A second resonance frequency where rail and sleepers mainly vibrate out of phase is around 1000 Hz. This resonance is to a large extent determined by rail pad properties. For the current set of track properties, the calculated pinned–pinned resonance frequency is 990 Hz. At this resonance, the rail vibrates with a wavelength equal to two sleeper bays with nodes above the sleepers. Since the second resonance frequency and the pinned–pinned

resonance frequency are so close, the low track receptance near sleepers (normally obtained at the pinned–pinned frequency) is shifted towards 1200 Hz. Similar track receptance curves for different sets of track properties are shown in Ref. [6].

The train is modelled as a single rigid mass corresponding to either a single driven wheelset of a passenger train ICM-III or a single driven wheelset of a 'Freight locomotive 1700'. Input data are listed in Table 1. Nominal traction forces are chosen to correspond to an ICM train with 3 cars including traction units, and a freight train with 2 locomotives and 20 wagons (total load 1200 tonnes), respectively.

A non-linear compressive stiffness of the wheel–rail contact is determined by assuming three-dimensional contact mechanics according to Hertz. The rail roughness profile, the wheel radius and the transverse profiles of rail and wheel define the time-variant contact geometry. The dimensions of the elliptical contact patch are calculated at each instant of time. Stationary rolling contact mechanics, according to Shen et al. [12], is adopted for the relationship between longitudinal creepage and longitudinal friction force. The friction coefficient is taken as 0.40. The applied driving torque on the wheelset is assumed to be constant [7]. The torque is chosen to correspond to the traction forces listed in Table 1. It was observed that the choice of nominal longitudinal creepage, as determined by the choice of nominal traction force (driving torque), was more critical to the predicted results than the choice of friction coefficient.

## 5. Initial roughness profile

An initial (low) level of railhead roughness, including a wide spectrum of different wavelengths, is present also on new rails. The simulation strategy is to account for such an initial roughness spectrum with wavelengths in the interval 10–100 mm. Depending on train speed, this will lead to a simultaneous train–track excitation at several frequencies within a given frequency range. The rail roughness level spectrum $L_r$ (Fig. 1(a)) is defined by

$$L_r = 10 \cdot_{10}\log\left\{\frac{\tilde{r}^2}{r_{ref}^2}\right\} \text{ [dB re 1 μm]}. \tag{1}$$

Here $\tilde{r}^2$ is the mean square value of the roughness profile $r(x)$ evaluated in 1/3 octave bands. In the simulations, the initial roughness profile is modelled as a sum of sine functions

$$r(x) = \sum_{i=1}^{M} a_i \left[\sum_{j=1}^{N} \sin\left(\frac{2\pi}{\lambda_{ij}}x + \phi_{ij}\right)\right]. \tag{2}$$

Wavelengths $\lambda_{ij}$ corresponding to $M$ bands with centre wavelengths $\lambda_i$ ranging from 10 to 100 mm are accounted for. The $N$ wavelengths in band $i$ are determined by assuming a constant wave-number increment $\Delta\kappa_i$ determined by the minimum and maximum wavelength in each band

$$\Delta\kappa_i = \frac{2\pi}{N}\left(\frac{1}{\lambda_i^{min}} - \frac{1}{\lambda_i^{max}}\right). \tag{3}$$

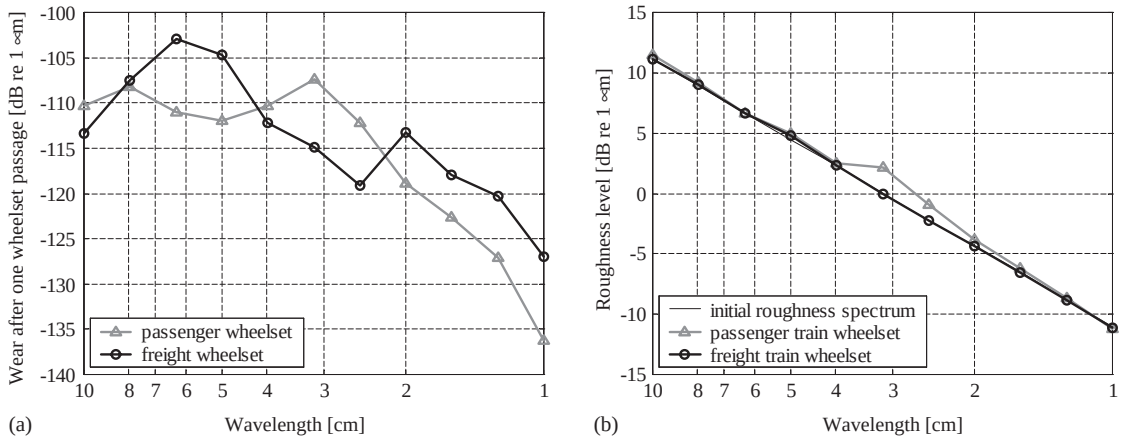


Fig. 4. (a) Influence of train model on calculated wear spectra after one driven wheelset passage. (b) Calculated roughness level spectra after 200,000 driven passenger wheelset passages or 30,000 driven freight wheelset passages. Initial spectrum and spectrum caused by freight traffic are overlapping.

In the simulations, the initial rail roughness level spectrum is chosen to correspond approximately to the measurements of a smooth rail [4]

$$L_{ri} = 22.1 \cdot_{10}\log(\lambda_i/0.01) - 11.0 \text{ [dB re 1 μm]}. \tag{4}$$

The initial roughness level spectrum is illustrated as the straight line in Fig. 4(b). The amplitude of the $N$ sines in each band is obtained as

$$a_i = \sqrt{\frac{2}{N}}\, 10^{L_{ri}/20} \text{ (μm)}. \tag{5}$$

By assigning phase angles to the sine functions that are uniformly and randomly distributed between 0 and $2\pi$, different roughness profiles defined by the same spectrum are generated. A filtering of the roughness profile to account for the size of the wheel–rail contact patch is performed at each instant of time. Each simulation with a given combination of track model, train model and roughness spectrum is carried out seven times with different sets of phase angles (roughness profiles).

## 6. Calculation of wear

The adopted hypothesis is that wear is caused by longitudinal slip due to driven wheelsets. The influence of lateral and spin creepage on wear is neglected as they are assumed to be small compared to the longitudinal creepage for a driven wheelset on tangent track. The material loss per unit area $\Delta m$ is assumed to be proportional to the frictional work density $w_f$

$$\Delta m(x,y) = C_w(x,y) w_f(x,y) = C_w \int p_f(x,y)\,\mathrm{d}t. \tag{6}$$

From the simulations carried out in conjunction with the present study, the wear coefficient $C_w$ was tuned to $2.5 \times 10^{-9}$ kg/N m. No local dependence of $C_w$ due, for example, to WEL, is

assumed here. The co-ordinate axes $x$ and $y$ describe the longitudinal and lateral directions of the contact patch, respectively. It is assumed that a point on the railhead stays within the contact patch during the time $\Delta t = 2a/v_c$, where $v_c$ is the speed with which the wheel–rail contact point moves along the rail. Assuming an elliptical contact patch with semi-axis lengths $a$ and $b$, the frictional power density $p_f$ is written as

$$p_f = \frac{P_f}{\pi ab} = \frac{vF_x\gamma_x}{\pi ab}. \tag{7}$$

Train speed, longitudinal friction force and longitudinal creepage are denoted by $v, F_x$ and $\gamma_x$, respectively. From Eqs. (6) and (7), the accumulated wear $\Delta r(x)$ at a position $x$ along the rail after one wheelset passage is obtained as

$$\Delta r(x) = \frac{\Delta m}{\rho} = \frac{C_w}{\rho}\frac{vF_x\gamma_x}{\pi ab}\frac{2a}{v_c}, \tag{8}$$

where $\rho$ is the mass density of the rail. Since the frictional power $P_f$ and the conditions of the contact patch are not constant during the time period $\Delta t$, the mean value of 20 wear calculations according to Eq. (8) with a time step of 0.01 ms is used. The wear is assigned to the centre of the distributed wear. This position is obtained by taking the wheel centre position and translating it by (1) the geometrical shift of the contact point due to the slope of the roughness profile and (2) the distance between the centre of the wear and the centre of the contact point [9].

## 7. Simulation scheme

The following scheme is adopted to predict a new rail roughness level spectrum after a given number of driven wheelset passages.

1. Generate a roughness profile by use of the adopted initial roughness spectrum and a set of random phase angles.
2. Calculate wear after one driven wheelset passage at each 0.5 mm along the rail.
3. Multiply wear by a chosen number of driven wheelset passages. Add to the initial roughness profile to obtain a new roughness profile.
4. Repeat steps 1–3 seven times with different sets of phase angles.
5. Calculate new roughness spectrum as the average of spectra corresponding to the new roughness profiles from seven simulations.

In each simulation, the evaluated length of the old and new roughness profiles corresponds to 20 sleeper bays. By repeating steps 1–5 with the new roughness spectrum as the initial roughness spectrum, rail roughness growth may be monitored with respect to time (number of driven wheelset passages). In the following, the calculated average of roughness growth evaluated over 140 ($7 \times 20$) sleeper bays will be presented. This should provide a sufficient statistical foundation for the present simulation model.

## 8. Validation of the model

The influence of train model on wear after one driven wheelset passage is illustrated in Fig. 4(a). For the passenger train model, a peak is obtained in the band around centre wavelength 3.2 cm. The location of this peak is explained by high frequency components of wheel–rail contact forces and frictional power caused by the combination of train speed 130 km/h and a low track receptance near the sleepers around 1200 Hz (see Fig. 3). When train speed is reduced to 80 km/h this peak is shifted towards centre wavelength 2 cm. The peak at approximately 6 cm for the freight train model is caused by the low track receptance around 400–600 Hz. The corresponding peak at 130 km/h is obtained at wavelength 8 cm.

Roughness level spectra after 1 year of traffic (200,000 driven passenger train wheelset passages or 30,000 driven freight train wheelset passages) are shown in Fig. 4(b). It is observed that the annual rail roughness growth caused by passenger traffic has a significantly larger impact on the shape of the roughness spectrum than the growth caused by 1 year of freight traffic. The agreement between simulations and measurements at the corrugated test site is good with respect to dominating wear wavelength and annual wear rate. By comparing the peak at approximately 4 cm in the measured roughness level spectra in Fig. 1(a) with the simulated results in Fig. 4, it is concluded that the simulation model seems capable of capturing the essential characteristics of the present damage mechanism.

The final profile after 1 year of traffic was calculated by use of two different approaches. In the first approach, the final profile was obtained by multiplying the calculated wear after one passenger wheelset passage by 200,000 and then adding it to the initial profile. Alternatively, growth of roughness was monitored by 8 consecutive simulations (each scaled by 25,000 wheelset passages) and using intermediate roughness profiles. Only small differences between the two approaches were observed. Thus, it seems acceptable to simulate the annual growth of rail roughness with only one simulation. In the simulations, it was also noted that although wear maxima seemed to appear at random positions along the rail depending on the initial roughness profile, areas with large wear were often observed near, but not directly above, the sleepers. This is in agreement with observations made in track.

## 9. Remedies to reduce roughness growth

A large rail roughness growth rate has been detected for wavelengths around 3.2 cm, see Fig. 4(b). This peak is explained by the low track receptance near the sleepers around 1200 Hz. The low receptance is primarily caused by the pinned–pinned resonance. From a structural dynamics point of view, there are a number of approaches to reduce the roughness growth.

### *9.1. Rail pad stiffness*

The pads at the current test sites are very stiff in comparison with modern resilient rail pads. An exchange to a softer pad will lead to reduced dynamic wheel–rail contact forces and a lower roughness growth rate in the entire investigated wavelength interval [13]. However, for a discretely supported track a local minimum in the track receptance will still remain near the sleepers around

the pinned–pinned resonance. Thus, the problem with a higher growth rate around 3.2 cm will only be partly solved.

### 9.2. Traffic load

Approximately 85% of all driven wheelsets passing the test site are fitted on passenger trains with constant speed 130 km/h. A less uniform traffic load (difference in rolling stock and train speeds) will distribute the wear to different wavelengths.

### 9.3. Rail cross-section and sleeper distance

The pinned–pinned resonance is shifted towards higher frequencies by increasing the size of the rail cross-section and/or by reducing sleeper distance (designing the track with a continuously supported rail will remove the pinned–pinned resonance). This means that, for a given train speed, a shorter roughness wavelength is needed to excite the pinned–pinned resonance. It has been shown that at very short wavelengths, say less than 20 mm, roughness growth is low because the finite size of the contact patch leads to a filtering of shorter wavelengths [6]. Thus, a proper combination of train speed and track properties may minimize the corrugation growth caused by the pinned–pinned resonance effect. It was observed that using a scatter in sleeper spacing has a negligible influence on roughness growth [13]. This was investigated by assigning a random sleeper spacing in the range $60 \pm 3.5$ cm in the track model. One possible solution to increase the track receptance above sleepers around the pinned–pinned resonance is to add damping to the rail. The added damping has the effect of smoothing peaks and troughs in the track receptance.

## 10. Concluding remarks

Railhead corrugation has been predicted through numerical simulation of dynamic train–track interaction in the time domain. The hypothesis is that wear is caused by longitudinal slip in the wheel–rail contact due to driven wheelsets, and that wear is proportional to longitudinal frictional power in the contact patch. The agreement between simulations and field observations is good with respect to dominating roughness wavelength and annual wear rate.

It is well known that two railway tracks with the same nominal design and traffic load do not in general show the same roughness growth. In fact, in the 'Silent Track' project two rails located only 250 m apart on the same tangent track showed a 15 dB difference in roughness level around a wavelength of 40 mm (although a peak in roughness level around 40 mm was observed at both sites). The roughness level at the smoother site was lower for all wavelengths investigated above around 7 mm. The only observed difference between the two sites was two different rail manufacturers. Strong evidence was found that the wear resistance of the rail plays an important role in the initiation and growth of corrugation [4]. Only the corrugated site was analyzed in the present case study.

Differences in steel production are known to influence the material structure, and consequently mechanical properties such as wear resistance and resistance to plastic deformation [5]. Such differences in mechanical properties of the rail have not yet been included in the present model. It

is possible that wear is not the single damage mechanism in the present case study. Furthermore, the different amounts of gauge corner wear that were observed at the two sites may lead to different contact geometries, and consequently differences in contact patch dimensions and contact stresses. One or several of these reasons may explain the difference in wear at the two 'Silent Track' test sites.

Improved wear and (elastic–plastic) material models are therefore called for to fully explain why some rails develop corrugation faster than others although the rails are exposed to the same nominal loading. When measured data on a locally dependent wear resistance are available, these can be accounted for in the present model. Depending on, for example, the curvature of the railhead irregularity, different wear coefficients can be assigned to corrugation peaks and troughs. The present train–track interaction model needs to be extended to account also for lateral interaction while maintaining the description of discrete sleeper supports. An important task for future research is to estimate the relative importance of different damage mechanisms.

## Acknowledgements

The current work was performed within the framework of the Brite/EuRam III project 'Silent Track'. The co-operation with Mr. Martin Hiensch, Dr. Edwin Verheijen and Mr. Pieter Dings of AEA Technology Rail in Utrecht, the Netherlands is acknowledged. AEA Technology Rail assembled the input data adopted in the train–track interaction model and supplied information on the traffic flow at the Dutch test site. Roughness data from the track is used by courtesy of NS Railinfrabeheer.

## References

[1] S. Grassie, J. Kalousek, Rail corrugations. Characteristics, causes and treatments, *Institute of Mechanical Engineers, Part F: Journal of Rail and Rapid Transit* 207 (1993) 57–68.

[2] J. Kalousek, S. Grassie, Rail corrugation: causes and cures, *International Railway Journal* (July 2000) 24–26.

[3] K. Knothe, Silent Track state-of-the-art study (chapter on roughness generation and growth models, availability restricted), Brite/EuRam III Silent Track, TU Berlin, 1997, 35pp.

[4] M. Hiensch, J.C.O. Nielsen, E. Verheijen, Rail corrugation in the Netherlands—measurements and simulations, *Wear* 253 (2002) 140–149.

[5] C.O. Frederick, A rail corrugation theory, *Proceedings of the Second International Conference on Contact Mechanics and Wear of Rail/Wheel Systems*, Kingston, RI, July 8–11, 1986, pp. 181–211.

[6] K. Hempelmann, Short pitch corrugation on railway rails—a linear model for prediction, VDI Fortschritt-Berichte, Düsseldorf, Reihe 12, No. 231, 1994, 147pp.

[7] A. Igeland, Dynamic Train/Track Interaction: Simulation of Railhead Corrugation Growth under a Moving Bogie Using Mathematical Models Combined with Full-Scale Measurements, Ph.D. Thesis, Department of Solid Mechanics, Chalmers University of Technology, Göteborg, Sweden, 1997.

[8] H. Ilias, Nichtlineare Wechselwirkungen von Radsatz und Gleis beim Überrollen von Profilstörungen, VDI Fortschritt Berichte, Düsseldorf, Reihe 12, No. 297, 1996.

[9] A. Igeland, H. Ilias, Rail head corrugation growth predictions based on non-linear high frequency vehicle/track interaction, *Wear* 213 (1997) 90–97.

[10] A. Böhmer, T. Klimpel, Plastic deformation of corrugated rails—a numerical approach using material data of rail steel, *Proceedings of the Fifth International Conference on Contact Mechanics and Wear of Rail/Wheel Systems,* Tokyo, July 25–28, 2000, pp. 58–65.

[11] J.C.O. Nielsen, A. Igeland, Vertical dynamic interaction between train and track—influence of wheel and track imperfections, *Journal of Sound and Vibration* 187 (5) (1995) 825–839.

[12] Z.Y. Shen, J.K. Hedrick, J.A. Elkins, A comparison of alternative creep force models for rail vehicle dynamic analysis, *Proceedings of the Eighth International Association for Vehicle System Dynamics (IAVSD) Symposium*, Cambridge, MA, 1983, pp. 591–605.

[13] J.C.O. Nielsen, Rail roughness generation and growth—influence of track parameters (availability restricted), Brite/EuRam III Silent Track, Chalmers University of Technology, Göteborg, Sweden, 1999, 22pp.